2015 IEEE International Conference on Robotics and Automation (ICRA)
Washington State Convention Center
Seattle, Washington, May 26-30, 2015

Feasible Center of Mass Dynamic Manipulability of Humanoid Robots

Yan Gu, C. S. George Lee, and Bin Yao†

Abstract— **Locomotion stability of a humanoid robot is closely related to the capacity to regulate its Center of Mass (CoM) motion. In this paper, the Feasible Center of Mass Dynamic Manipulability (FCDM) is introduced and analyzed as a measure of this capacity. The effects of posture, joint velocities and gravity on the torque-bounded dynamic manipulability ellipsoid are first analyzed on an n-DOF planar humanoid robot with single-foot support. The ellipse orientation has a linear relationship with the ankle angle, and its shape is independent on the ankle angle. Furthermore, three common and important ground-contact constraints - the unilateral contact-force constraint, the friction constraint, and the Center of Pressure constraint - are incorporated in the derivation of FCDM. It shows geometrically how each of the three constraints shrinks the original torque-bounded manipulability polytope and affects the maximum achievable CoM acceleration in different directions. Finally, a push recovery task was simulated to show that a robot's posture affects the feasible range of the CoM acceleration in a specific direction.**

I. Introduction

Maintaining balance of humanoid locomotion is challenging due to underactuation and various ground-contact constraints. Different balance criteria have been proposed to address this problem. Among them, the most frequently used one is the Zero Moment Point (ZMP) balance criterion [1], [2]. It requires that the ZMP should always be kept strictly within the support polygon. Another balance criterion based on the Foot Rotation Indicator (FRI) [3] essentially requires no foot rotation. In addition, the balance criterion associated with the Centroidal Moment Pivot (CMP) [4], also known as the Zero Rate of change of Angular Momentum (ZRAM) [5], can be used to guarantee no angular motion around a robot's CoM.

Locomotion stability of a humanoid robot is defined as the ability not to fall over [6]. According to this definition, humanoid locomotion stability is closely related to the ability to regulate a robot's CoM motion, and none of the above-mentioned balance criteria indicates such the ability and thus they may not be suitable for instability prediction. Wieber [7] first introduced the concept of viability [8] as a necessary and sufficient measure for humanoid locomotion stability. Later on, capturability [9] was proposed as a computationally less expensive approximation of viability. A state is N-step capturable if and only if the robot is able to come to a complete stop by taking N or fewer steps from this state. The argument behind capturability is that the ability to come to a complete stop is a good approximation of the ability to avoid falling.

†Yan Gu and Bin Yao are with the School of Mechanical Engineering, and C. S. George Lee is with the School of Electrical and Computer Engineering, Purdue University, West Lafayette, IN 47907, U.S.A. {gu49, csglee, byao}@purdue.edu

‡This work was supported in part by the National Science Foundation under Grant IIS-0916807. Any opinion, findings, and conclusions or recommendations expressed in this material are those of the authors and do not necessarily reflect the views of the National Science Foundation.

Since the ability to regulate CoM motion is key to humanoid locomotion stability, it is natural to analyze, evaluate and take advantage of the CoM acceleration capacity of a humanoid robot. Dynamic manipulability [10], an evaluation index for the dynamic performance of a robot manipulator, provides a geometric interpretation of the manipulator end-effector's acceleration capacity at a given posture. Naksuk and Lee [11] introduced the ZMP manipulability ellipsoid of a humanoid robot based on the concept of dynamic manipulability and the ZMP balance criterion. However, necessary ground-contact constraints such as the friction constraint and the unilateral constraint were not considered. Hence, the feasibility of the ellipsoid is not guaranteed. Cotton *et al.* derived the CoM dynamic manipulability polytope of a humanoid robot [12]. The ZMP balance criterion (i.e., the Center of Pressure (CoP) constraint) was considered to obtain the maximal isotropic CoM acceleration within the CoM dynamic manipulability polytope without including other ground-contact constraints.

In this paper, we propose a new index to analyze and evaluate the CoM acceleration capacity of a humanoid robot at a given posture, called Feasible CoM Dynamic Manipulability (FCDM). The FCDM indicates the ability of a humanoid robot to regulate its CoM motion at a given posture under ground-contact constraints. To our best knowledge, there seems to be no previous related research that geometrically analyzed the effects of ground-contact constraints on the feasible CoM dynamic manipulability of a humanoid robot. Also, the CoM acceleration capacity of a humanoid robot in different directions was not analyzed. In this paper, the CoM dynamic manipulability ellipsoid is revisited in Section II, and the effects of posture, joint velocities and gravity on the ellipsoid are analyzed with results applicable to both robot manipulators and humanoid robots. Section III introduces the feasible CoM dynamic manipulability by incorporating three common ground-contact constraints. The effects of the ground-contact constraints on the achievable CoM acceleration in different directions are studied, both analytically and numerically. Moreover, the posture of a humanoid robot is optimized to achieve the maximum CoM acceleration along a given direction. The optimization result is adopted as the initial configuration for a push recovery task in Section IV.

II. CoM Dynamic Manipulability Ellipsoid

In this section, the CoM dynamic manipulability [11], [12] is revisisted. Here, only the flat-footed single-support case is considered.

With the support foot assigned as the base link, the dynamics of an n-DOF planar robot can be written as

$$\mathbf{A}(\mathbf{q})\ddot{\mathbf{q}}(t)+\mathbf{h}(\mathbf{q},\dot{\mathbf{q}})+\mathbf{c}(\mathbf{q})=\boldsymbol{\tau}(t) \tag{1}$$

where $\mathbf{q}=[q_1,q_2,\ldots,q_n]^T\in\mathbb{R}^n$, $\dot{\mathbf{q}}=[\dot{q}_1,\dot{q}_2,\ldots,\dot{q}_n]^T\in\mathbb{R}^n$, and $\ddot{\mathbf{q}}=[\ddot{q}_1,\ddot{q}_2,\ldots,\ddot{q}_n]^T\in\mathbb{R}^n$ are the joint-variable vector, the joint-velocity vector, and the joint-acceleration vector of the robot, respectively, $\mathbf{A}(\mathbf{q})\in\mathbb{R}^{n\times n}$ is the inertia matrix, $\mathbf{h}(\mathbf{q},\dot{\mathbf{q}})\in\mathbb{R}^n$ is the Coriolis and centrifugal force vector, $\mathbf{c}(\mathbf{q})\in\mathbb{R}^n$ is the gravitational force term, and $\boldsymbol{\tau}=[\tau_1,\tau_2,\ldots,\tau_n]^T\in\mathbb{R}^n$ is the joint-torque vector.

The relationship between the CoM velocity and the joint velocities via the CoM Jacobian is

$$\dot{\mathbf{r}}_c=\mathbf{J}_c(\mathbf{q})\dot{\mathbf{q}} \tag{2}$$

where $\mathbf{r}_c=[x_c,y_c,z_c]^T$ is the CoM location and $\mathbf{J}_c(\mathbf{q})$ is the CoM Jacobian. Taking the time derivative of Eq. (2) and combining it with Eq. (1), the CoM acceleration can be obtained as

$$\ddot{\mathbf{r}}_c=\mathbf{J}_c\mathbf{A}^{-1}(\boldsymbol{\tau}-\mathbf{h}-\mathbf{c})+\dot{\mathbf{J}}_c\dot{\mathbf{q}}\overset{\triangle}{=}\mathbf{a}_{c\tau}+\mathbf{a}_{cv}+\mathbf{a}_{cg}\equiv\mathbf{a}_c \tag{3}$$

where $\mathbf{a}_c=\ddot{\mathbf{r}}_c$, $\mathbf{a}_{c\tau}=\mathbf{J}_c\mathbf{A}^{-1}\boldsymbol{\tau}$, $\mathbf{a}_{cv}=-\mathbf{J}_c\mathbf{A}^{-1}\mathbf{h}+\dot{\mathbf{J}}_c\dot{\mathbf{q}}$, and $\mathbf{a}_{cg}=-\mathbf{J}_c\mathbf{A}^{-1}\mathbf{c}$.

At a given posture, $\mathbf{a}_{c\tau}$, $\mathbf{a}_{cv}$ and $\mathbf{a}_{cg}$ are determined by the joint torques, the joint velocities and the gravity term, respectively. In the following, the effects of these three sets of variables on the achievable set of CoM acceleration at a given posture are analyzed.

To analyze the effect of the joint-torque limit, we consider $\boldsymbol{\tau}\in[-\boldsymbol{\tau}_{max},\boldsymbol{\tau}_{max}]$, where $\boldsymbol{\tau}_{max}=[\tau_{max1},\tau_{max2},...,\tau_{maxn}]^T$, and $\mathbf{J}_c\mathbf{A}^{-1}\boldsymbol{\tau}$ can be rewritten as $\mathbf{J}_c\mathbf{A}^{-1}\mathbf{W}\boldsymbol{\tau}_N$, where $\mathbf{W}=\text{diag}[\tau_{max1},\tau_{max2},...,\tau_{maxn}]$ is a scaling matrix and $\boldsymbol{\tau}_N=[\tau_{N1},\tau_{N2},...\tau_{Nn}]^T$ is the normalized joint-torque vector with $|\tau_{Ni}|\leq 1$, $i=1,2,\ldots,n$. Denoting $\tilde{\mathbf{J}}=\mathbf{J}_c\mathbf{A}^{-1}\mathbf{W}$ and applying singular value decomposition, $\tilde{\mathbf{J}}$ can be decomposed into $\tilde{\mathbf{J}}=\mathbf{U}\Sigma\mathbf{V}^T$, where $\mathbf{U}=[\mathbf{u}_1,\mathbf{u}_2,\mathbf{u}_3]\in\mathbb{R}^{3\times 3}$ and $\mathbf{V}=[\mathbf{v}_1,\mathbf{v}_2,\ldots,\mathbf{v}_n]\in\mathbb{R}^{n\times n}$ are orthogonal matrices and

$$\Sigma=\left[\begin{array}{ccc|c}\sigma_1 & 0 & 0 & \\ 0 & \sigma_2 & 0 & \mathbf{0}_{3\times(n-3)}\\ 0 & 0 & \sigma_3 & \end{array}\right]$$

where $\Sigma\in\mathbb{R}^{3\times n}$ with singular values in a descending order.

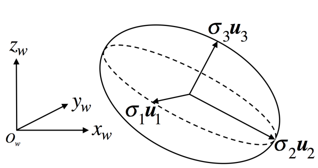

Fig. 1: CoM Dynamic Manipulability Ellipsoid.

$\tilde{\mathbf{J}}$ maps the sphere $||\boldsymbol{\tau}_N||\leq 1$ onto an ellipsoid (see Fig. 1) in the CoM acceleration space, which is the CoM Dynamic Manipulability Ellipsoid. The ellipsoid semi-principal axes are of length σ_1, σ_2 and σ_3 in the directions of $\mathbf{u}_1$, $\mathbf{u}_2$ and $\mathbf{u}_3$, respectively. Although the complete torque-bounded set of CoM acceleration at a given posture with given joint velocities is not an ellipsoid but a polytope, which is bounded by $|\tau_{Ni}|\leq 1$, $i=1,2,\ldots,n$, the ellipsoid is a reasonable approximation [10] and it shares the same center as the polytope. From Eq. (3), it is clear that the shape and the orientation of the ellipsoid/polytope are affected by the robot's posture and that the center of the ellipsoid/polytope at a given posture is determined by joint velocities and gravity.

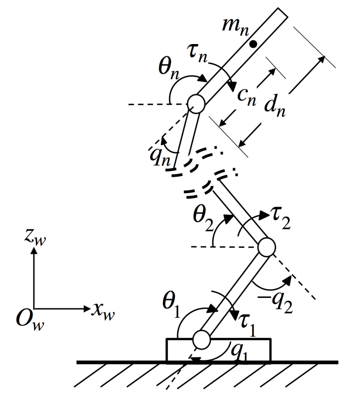

Fig. 2: An n-DOF Planar Robot.

A. *Effects of Posture on the Shape and Orientation of the CoM Dynamic Manipulability Ellipsoid*

The posture adopted by a humanoid robot can greatly affect its achievable maximum CoM acceleration in a specific direction. Here, a planar robot in the sagittal plane with only revolute joints is considered (see Fig. 2). $\boldsymbol{\theta}=[\theta_1,\ldots,\theta_n]^T\in\mathbb{R}^n$ is the link angle of the robot with respect to the world coordinate frame with $\theta_i=\sum_{k=1}^{i}q_k$. The CoM dynamic manipulability ellipsoid then becomes an ellipse. It can be proved that the ankle joint q_1 does not affect the lengths of the ellipse semi-principal axes and hence the shape of the ellipse. Also, the orientation of the ellipse varies linearly with the ankle joint when other joint angles are fixed. Due to the space limitation, detailed proof is omitted. Simulation results with zero joint velocities (see Fig. 3) showed the independence of the ellipse shape on the first joint angle and the linear relationship between the first joint angle and the ellipse orientation α.

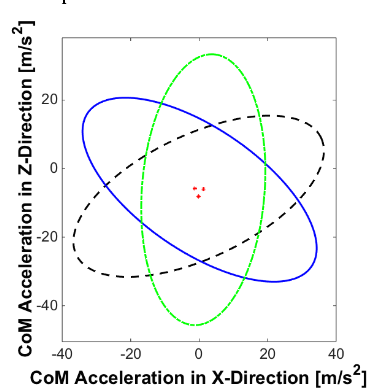

Fig. 3: Linear Effect of the Ankle Joint on the Ellipse Orientation and Independence of the Ellipse Shape on the Ankle Joint (black dash: $q_1=0°$, $\alpha=26°$; blue solid: $q_1=60°$, $\alpha=-34°$; green dot-dash: $q_1=120°$, $\alpha=-94°$).

B. Effects of Joint Velocities and Gravity on the Center of the CoM Dynamic Manipulability Ellipsoid

The center of the CoM dynamic manipulability ellipsoid/polytope at a given posture is determined by the joint velocities and gravity. In [13], it provides an analytic approach to evaluate the magnitude of the velocity effect. Note that $\mathbf{J}_c\mathbf{A}^{-1}\mathbf{h}$ and $\dot{\mathbf{J}}_c\dot{\mathbf{q}}$ can both be written in a quadratic form as

$$\mathbf{J}_c\mathbf{A}^{-1}\mathbf{h} = \begin{bmatrix} \dot{\mathbf{q}}^T\mathbf{H}_{v1}(\mathbf{q})\dot{\mathbf{q}} \\ \dot{\mathbf{q}}^T\mathbf{H}_{v2}(\mathbf{q})\dot{\mathbf{q}} \\ \dot{\mathbf{q}}^T\mathbf{H}_{v3}(\mathbf{q})\dot{\mathbf{q}} \end{bmatrix} \text{ and } \dot{\mathbf{J}}_c\dot{\mathbf{q}} = \begin{bmatrix} \dot{\mathbf{q}}^T\mathbf{J}_{v1}(\mathbf{q})\dot{\mathbf{q}} \\ \dot{\mathbf{q}}^T\mathbf{J}_{v2}(\mathbf{q})\dot{\mathbf{q}} \\ \dot{\mathbf{q}}^T\mathbf{J}_{v3}(\mathbf{q})\dot{\mathbf{q}} \end{bmatrix} \quad (4)$$

where $\mathbf{H}_{vi}$ and $\mathbf{J}_{vi}$ $(i = 1,2,3)$ are known and bounded matrices of $\mathbf{q}$. Hence, at a given posture $\mathbf{a}_{cv}$ is bounded:

$$||\mathbf{a}_{cv}||_2 = ||-\mathbf{J}_c\mathbf{A}^{-1}\mathbf{h} + \dot{\mathbf{J}}_c\dot{\mathbf{q}}||_2 \le \beta(\mathbf{q})||\dot{\mathbf{q}}||_2^2, \quad (5)$$

where β is a known function of $\mathbf{q}$. The gravity effect at a given posture $\mathbf{q}$ can be directly computed from

$$||\mathbf{a}_{cg}||_2 = ||-\mathbf{J}_c\mathbf{A}^{-1}\mathbf{c}||_2. \quad (6)$$

III. Feasible CoM Dynamic Manipulability

Different from a fixed-based robot manipulator, humanoid locomotion is subject to various ground-contact constraints. These constraints decide the feasible subset of the torque-bounded CoM dynamic manipulability polytope. This feasible subset is defined as the Feasible CoM Dynamic Manipulability (FCDM) Polytope. Here, three common ground-contact constraints in humanoid locomotion are considered, including 1) the unilateral ground-contact constraint, 2) the friction constraint, and 3) the CoP constraint (i.e., the ZMP balance criterion). They are mathematically and respectively described as:

$$\begin{aligned} &1) \quad F_z \ge 0 \\ &2) \quad \sqrt{F_x^2 + F_y^2} \le \mu|F_z| \\ &3) \quad \mathbf{r}_p \in \{SP\} \setminus \partial\{SP\} \end{aligned} \quad (7)$$

where F_x, F_y and F_z are the x-, y- and z-components of the ground reaction force $\mathbf{F}_R$, respectively, μ is the friction coefficient, $\mathbf{r}_p = [x_p, y_p, 0]^T$ is the CoP/ZMP location on the horizontal even terrain, $\{SP\}$ is the support polygon, and $\partial\{SP\}$ is the boundary of $\{SP\}$.

To analyze the effects of the above constraints, a planar humanoid robot (see Fig. 4) is considered. Combined with the unilateral constraint, the friction constraint becomes

$$-\mu F_z \le F_x \le \mu F_z. \quad (8)$$

Since $F_x = M\ddot{x}_c$ and $F_z = M\ddot{z}_c + Mg$ ($g = 9.81$ m/s^2 and M is the total mass), the set of achievable CoM acceleration bounded by the friction constraint is then described by

$$-\mu(\ddot{z}_c + g) \le \ddot{x}_c \le \mu(\ddot{z}_c + g). \quad (9)$$

For a planar robot, the CoP constraint becomes $x_0 < x_p < x_0 + d_f$, where x_0 is the heel location and d_f is the length of the support foot. The CoP location in the x-direction [14] is

$$x_p = x_0 + h_f + \frac{m_f g c_f - \tau_1 - M\ddot{x}_c t_f}{M(g + \ddot{z}_c)} \quad (10)$$

where m_f, c_f, h_f and t_f are the mass, ankle-CoM distance, ankle-heel distance and height of the support foot, respectively, and -τ_1 is the joint torque applied to the support foot (see Fig. 4). Combined with the unilateral constraint, the subset of the achievable CoM acceleration bounded by the CoP constraint then becomes

$$0 < \frac{m_f g c_f - \tau_1 - M\ddot{x}_c t_f}{M(g + \ddot{z}_c)} + h_f < d_f. \quad (11)$$

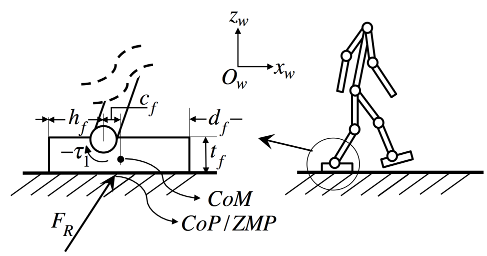

Fig. 4: Support Foot Geometry.

A. Effects of Ground-Contact Constraints on the Achievable CoM Acceleration at a Given Posture

From Eq. (9), it is clear that the subset bounded by the friction constraint only depends on the friction coefficient. However, Eq. (11) indicates that the subset bounded by the CoP constraint is dependent on the given posture and the torque limit. Therefore, it is not straightforward to determine how the CoP constraint shrinks the original torque-bounded polytope geometrically. The FCDM polytopes for two planar robots with zero joint velocities are shown in Fig. 5.

Figure 5 shows that the friction constraint is indeed not affected by the torque constraint or the posture because the corresponding boundaries in two cases are the same. Also, the 3-DOF robot at the given posture has a relatively larger subset bounded by the CoP constraint compared with the 2-DOF robot. It indicates that the higher DOF may have higher capacity to regulate CoM acceleration.

From Fig. 5 we can also see that the achievable CoM acceleration in different directions is drastically different due to the existence of the ground-contact constraints. Previous research on evaluation of a robot's dynamic performance is more focused on the global performance [15], [16]. Here, our interest is in the maximum achievable CoM acceleration in a specific direction. Thus, it is necessary to first analyze the effects of ground-contact constraints on the maximum achievable CoM acceleration in different directions. The following analysis is based on Fig. 5(b).

1) Horizontal Direction: When the CoM acceleration is exactly horizontal, its magnitude is at most μg due to the friction constraint. It also indicates that the CoM acceleration in this case may be realized by an infinite number of postures for a redundant robot.

2) Downward Direction: The vertical downward CoM acceleration is at most g in magnitude, which is determined by the unilateral constraint. For general downward acceleration, its magnitude is bounded by the friction constraint (implicitly with the unilateral constraint). There may exist infinitely many postures for CoM acceleration maximization.

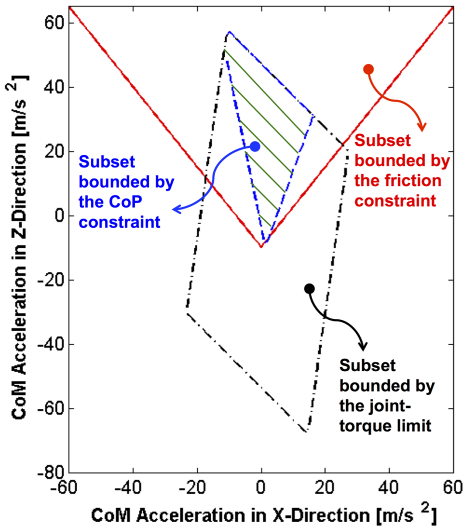

(a) FCMP of a 2-DOF Planar Humanoid Robot.

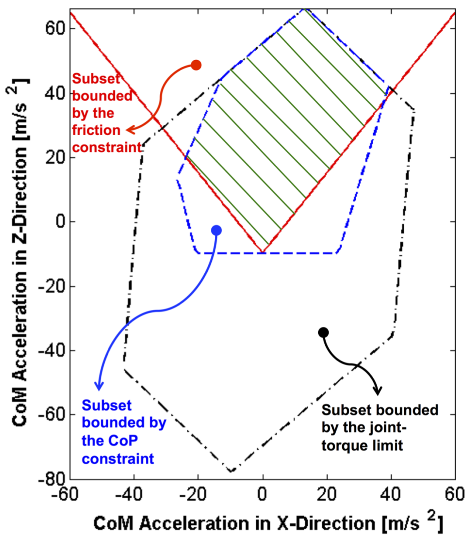

(b) FCMP of a 3-DOF Planar Humanoid Robot.

Fig. 5: Feasible CoM Dynamic Manipulability Polytopes (FCMP) (black dot-dash: boundary of the subset bounded by the joint-torque limit; red solid: boundary of the subset bounded by the friction constraint (implicitly with the unilateral constraint); blue dash: boundary of the subset bounded by the CoP constraint (implicitly with the unilateral constraint and the joint-torque limit); green shaded: subset bounded by the joint-torque limit and the three ground-contact constraints; that is, FCMP).

3) Upward Direction: The upward CoM acceleration is bounded by the CoP constraint (implicitly with the joint-torque constraint) and the friction constraint. For the directions bounded by the friction constraint, an infinite number of postures may exist for maximization of CoM acceleration. For the directions bounded by the CoP constraint, a unique optimal posture may exist.

B. Numerical Posture Search for Maximum Feasible CoM Acceleration in Different Directions

The optimal posture that results in the maximum CoM acceleration in a specified direction can be found numerically by solving the following optimization problem:

$$\begin{aligned} &\max ||\ddot{\mathbf{r}}_c(\mathbf{q},\boldsymbol{\tau})|| \\ \text{subject to } &\mathbf{q} \in [\mathbf{q}_{min}, \mathbf{q}_{max}] \\ &\boldsymbol{\tau} \in [-\boldsymbol{\tau}_{max}, \boldsymbol{\tau}_{max}] \\ &\dot{\mathbf{q}} = \dot{\mathbf{q}}_0 \\ &\ddot{\mathbf{r}}_c = \mathbf{J}_c\mathbf{A}^{-1}(\boldsymbol{\tau}-\mathbf{h}-\mathbf{c}) + \dot{\mathbf{J}}_c\dot{\mathbf{q}} \\ &F_z \geq 0 \\ &\sqrt{F_x^2+F_y^2} \leq \mu|F_z| \\ &\mathbf{r}_p \in \{SP\} \setminus \partial\{SP\} \\ &\angle(\ddot{\mathbf{r}}_c) = \gamma \end{aligned} \tag{12}$$

where γ specifies the desired direction of the CoM acceleration and $\dot{\mathbf{q}}_0$ is the given joint velocities.

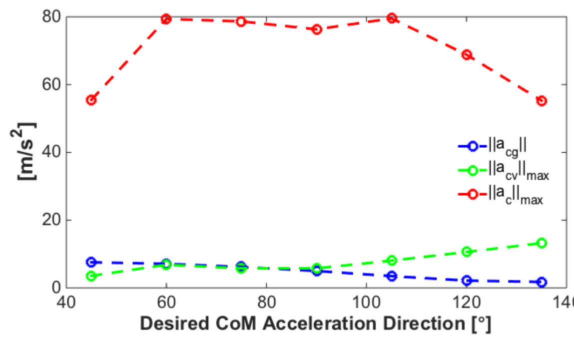

Fig. 7: Maximum Feasible CoM Acceleration at the Optimal Postures in Fig. 6(a).

Simulation results on a planar robot confirmed the previous analysis. The maximum feasible CoM acceleration bounded by the friction constraint can be achieved by an infinite number of postures. For each of the other directions, there exists a unique optimal posture. Figure 6(a) shows the optimal postures for seven of those directions. The maximum feasible CoM acceleration in each of those seven directions is shown in Fig. 7 (red line). The blue line in Fig. 7 shows the magnitude of the corresponding gravity-influenced component $\mathbf{a}_{cg}$ computed based on Eq. (6). According to Eq. (5), the magnitude of the joint-velocity induced component $\mathbf{a}_{cv}$ at a given posture is bounded. Because the joint-velocity variable $\dot{\mathbf{q}}_0$ is set to zero in the optimization, the upper bound of the joint-velocity induced component $\mathbf{a}_{cv}$ is computed with $||\dot{\mathbf{q}}|| \leq \pi$ rad/s (see Fig. 7 green line).

From Figs. 6-7, we discover that:

- The maximum CoM acceleration in the upward direction as shown in Fig. 6(a) seems to be achieved when the hip joint is close to singularity;
- Because the changes of both the knee and the hip angles are relatively small at different optimal postures as shown in Fig. 6(a), the ellipse orientation seems to change with the ankle angle monotonically;
- The major axis of the torque-bounded ellipse aligns approximately with the specified CoM acceleration direction (see Fig. 6(b));
- $||\mathbf{a}_{cg}||$ is relatively small at the optimal postures for different directions as shown in Fig. 6(a) possibly

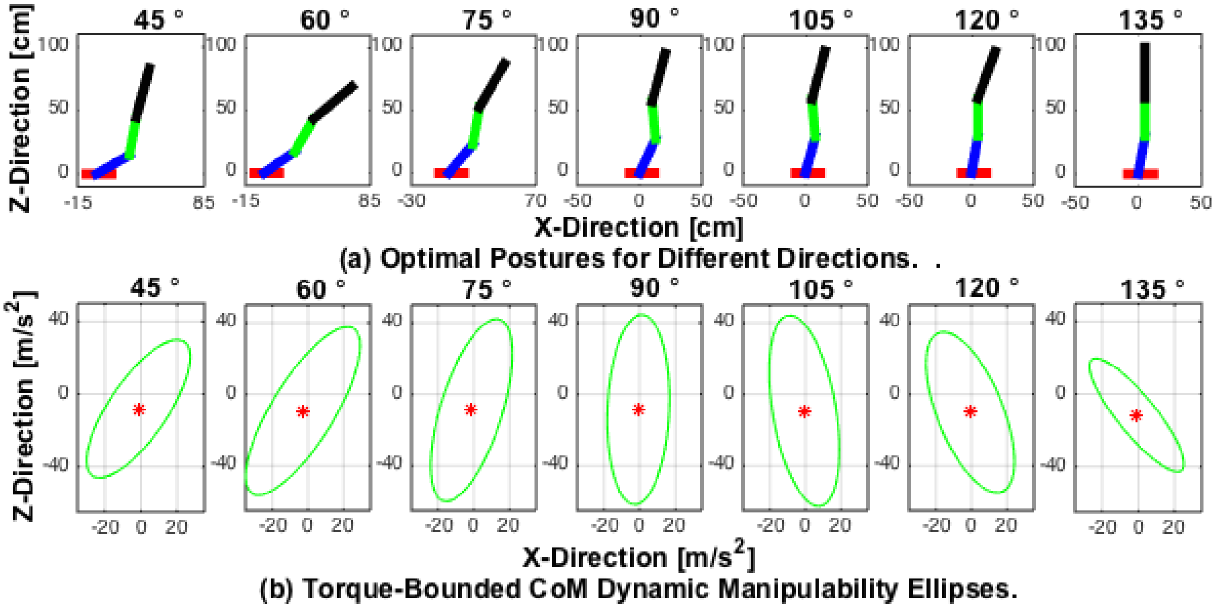

Fig. 6: Optimal Postures for Achieving Maximum Feasible CoM Acceleration in Different Directions and Corresponding Torque-Bounded CoM Dynamic Manipulability Ellipses (Specified CoM Acceleration Directions (from left to right): 45°, 60°, 75°, 90°, 105°, 120°, 135°).

because it requires relatively less actuation power to hold the robot weight near singularity [17];

- The translational effect of the joint velocities on the ellipse center is relatively small in magnitude compared to $||a_c||_{max}$; however, it may induce a significant change of the achievable maximum CoM acceleration in the specified direction [13].

IV. Push Recovery at a Standing Posture

A. Problem Formulation

In this section, a standing posture, selected by the numerical optimization in Section III-B, is adopted as the initial posture for a push recovery task. For simplicity, a planar robot with two revolute joints is simulated. The robot is static before the push and the instantaneous push is known. Also, the initial CoM velocity right before the push is relatively small so that the robot is able to recover from the push with little posture change. The simulation results are compared with another initial posture at which the achievable CoM deceleration in the push direction is much smaller. A nonlinear model predictive controller (NMPC) [18] is designed.

The state and the control input are chosen to be $\mathbf{x} = [\theta_1, \theta_2, \dot{\theta}_1, \dot{\theta}_2]^T$ and $\boldsymbol{\tau} = [\tau_1, \tau_2]^T$, respectively. The optimal control problem over a finite horizon N at time step k is formulated as

$$\min_{\boldsymbol{\tau}^*} \sum_{i=k}^{k+N-1} (\mathbf{x}_{\tau i}^T \mathbf{P} \mathbf{x}_{\tau i} + \boldsymbol{\tau}_i^{*T} \mathbf{Q} \boldsymbol{\tau}_i^*) \tag{13}$$

$$\text{subject to} \quad \mathbf{x}_{\tau i} \in [\mathbf{q}_{min}, \mathbf{q}_{max}]$$
$$\boldsymbol{\tau}_i^* \in [-\boldsymbol{\tau}_{max}, \boldsymbol{\tau}_{max}]$$
$$f(\mathbf{x}_{\tau i}, \boldsymbol{\tau}_i^*) \leq \mathbf{0}$$

where $\mathbf{x}_{\tau i}$ is the predicted state at time step i, $\boldsymbol{\tau}_i^*$ is the admissible control input at time step i, $\mathbf{P}$ and $\mathbf{Q}$ are hand-tuned semi-positive-definite and positive-definite weighting matrices, respectively, and $f(\mathbf{x}_{\tau i}, \boldsymbol{\tau}_i^*) \leq \mathbf{0}$ represents a set of linear constraints including the full dynamics and the ground-contact constraints. The hand-tuned parameters are chosen as $N = 3$, $\mathbf{P}$ =diag$[0, 0, 10^4, 10^4]$, and $\mathbf{Q}$ =diag$[0.1, 0.1]$.

B. Simulation Results

Simulation results are shown in Fig. 8 and Fig. 9. The initial CoM velocity $\dot{\mathbf{r}}_{c0}$ after a gentle push in both cases is horizontal in the positive x-direction, and $\dot{\mathbf{r}}_{c0} = [7.85$ cm/s$, 0]^T$. The maximum CoM acceleration in the negative x-direction at Posture 1 and Posture 2 is 7.85 m/s^2 and 0.74 m/s^2, respectively. Simulation results show that the robot in Example 1 is recovered from the push in 4 time steps (see Fig. 8) while in Example 2 (see Fig. 9) the recovery time is 14 time steps. It verified that a robot's posture can indeed affect its maximum feasible CoM acceleration, and thus the posture should be carefully selected.

V. Conclusion

In this paper, we have introduced the concept of Feasible CoM Dynamic Manipulability for analysis and evaluation of the CoM acceleration capacity of a humanoid robot subject to ground-contact constraints. By analyzing the torque-bounded CoM dynamic manipulability ellipsoid of a planar n-DOF humanoid robot, it was analytically found that the orientation of the ellipse is dependent on the ankle joint linearly and that the ankle joint does not affect the shape of the ellipse. Also, the joint velocities and the gravitational force have a translational effect on the ellipsoid center. For a walking humanoid robot in the single-support phase, three common ground-contact constraints were incorporated to generate the feasible CoM dynamic manipulability polytope at a specific posture. The effects of the constraints on the

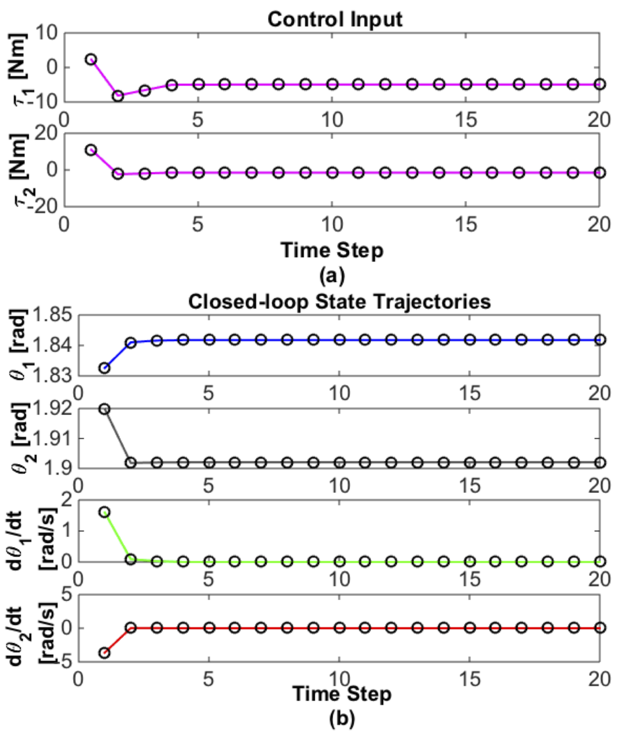

Fig. 8: Example 1: Push Recovery with an initial posture $[\theta 1, \theta 2]^T = [105°, 110°]^T$ (1 time step=0.01 s).

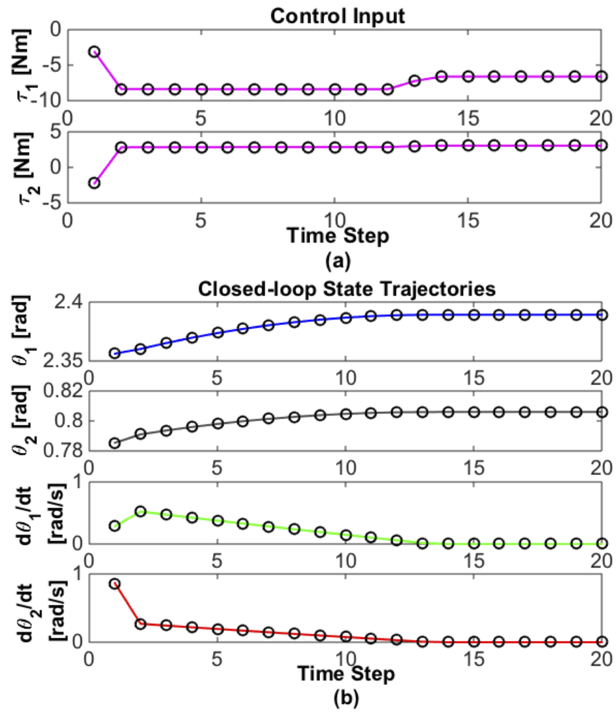

Fig. 9: Example 2: Push Recovery with an initial posture $[\theta 1, \theta 2]^T = [135°, 45°]^T$ (1 time step=0.01 s).

maximum achievable CoM acceleration in different directions were analyzed on a planar humanoid robot with results that are extendable to a spatial humanoid robot. The best posture to achieve the maximum CoM acceleration in a given direction can be found by utilizing the proposed numerical optimization. The selected optimal posture was applied to a humanoid robot in a push recovery task. Simulation results verified that the initial posture indeed greatly affects the recovery time.

Results in this paper are helpful in deciding the optimal posture of a humanoid robot to achieve maximum acceleration in a specific direction. It might also provide a useful analysis tool for the actuator design of a humanoid robot. Most of the results applicable to planar robots in this study can also be extended to spatial humanoid robots.

References

[1] M. Vukobratovic, A. A. Frank, and D. Juricic, “On the stability of biped locomotion,” *IEEE Trans. Biomed. Eng.*, vol. 17, no. 1, pp. 25–26, January 1970.

[2] M. Vukobratović and B. Borovac, “Zero-moment point–thirty five years of its life,” *Int. J. Humanoid Robotics*, vol. 1, no. 01, pp. 157–173, 2004.

[3] A. Goswami, “Foot rotation indicator (FRI) point: A new gait planning tool to evaluate postural stability of biped robots,” in *Proc. 1999 IEEE Int. Conf. Robotics and Automation*, pp. 47–52.

[4] M. Popovic, A. Hofmann, and H. Herr, “Angular momentum regulation during human walking: biomechanics and control,” in *Proc. 2004 IEEE Int. Conf. Robotics and Automation*, pp. 2405–2411.

[5] A. Goswami and V. Kallem, “Rate of change of angular momentum and balance maintenance of biped robots,” in *Proc. 2004 IEEE Int. Conf. Robotics and Automation*, pp. 3785–3790.

[6] J. Pratt and R. Tedrake, “Velocity-based stability margins for fast bipedal walking,” in *Fast Motions in Biomechanics and Robotics*. Springer, 2006, pp. 299–324.

[7] P. Wieber, “On the stability of walking systems,” in *Proc. Int. Workshop Humanoid and Human Friendly Robotics*, 2002.

[8] J. P. Aubin, *Viability theory*. Springer, 2009.

[9] T. Koolen, T. De Boer, J. Rebula, A. Goswami, and J. Pratt, “Capturability-based analysis and control of legged locomotion, Part 1: Theory and application to three simple gait models,” *Int. J. Robotics Research*, vol. 31, no. 9, pp. 1094–1113, 2012.

[10] T. Yoshikawa, “Dynamic manipulability of robot manipulators,” in *Proc. 1985 IEEE Int. Conf. Robotics and Automation*, pp. 1033–1038.

[11] N. Naksuk and C. S. G. Lee, “Zero moment point manipulability ellipsoid,” in *Proc. 2006 IEEE Int. Conf. Robotics and Automation*, pp. 1970–1975.

[12] S. Cotton, P. Fraisse, and A. P. Murray, “On the manipulability of the center of mass of humanoid robots: application to design,” in *2010 ASME Int. Design Eng. Tech. Conf. and Comput. and Inform. Eng. Conf.*, pp. 1259–1267.

[13] M. Rosenstein and R. A. Grupen, “Velocity-dependent dynamic manipulability,” in *Proc. 2002 IEEE Int. Conf. Robotics and Automation*, pp. 2424–2429.

[14] Y. Pai and K. Iqbal, “Simulated movement termination for balance recovery: can movement strategies be sought to maintain stability in the presence of slipping or forced sliding?” *J. Biomechanics*, vol. 32, no. 8, pp. 779–786, 1999.

[15] T. J. Graettinger and B. H. Krogh, “The acceleration radius: a global performance measure for robotic manipulators,” *IEEE J. Robotics and Automation*, vol. 4, no. 1, pp. 60–69, 1988.

[16] A. Bowling and C. H. Kim, “Dynamic performance analysis for non-redundant robotic manipulators in contact,” in *Proc. 2003 IEEE Int. Conf. Robotics and Automation*, pp. 4048–4053.

[17] C. Wang, W. Timoszyk, and J. Bobrow, “Payload maximization for open chained manipulators: finding weightlifting motions for a Puma 762 robot,” *IEEE Trans. Robot. Autom.*, vol. 17, no. 2, pp. 218–224, 2001.

[18] L. Grüne and J. Pannek, *Nonlinear model predictive control*. Springer, 2011.